CHEMISTRY
A EUROPEAN JOURNAL

DOI: 10.1002/chem.200600571

Enhancement of Relaxivity Rates of Gd–DTPA Complexes by Intercalation into Layered Double Hydroxide Nanoparticles

Zhi Ping Xu,[a] Nyoman D. Kurniawan,[b, c] Perry F. Bartlett,[b] and Gao Qing Lu*[a]

Abstract: In this paper we report the preparation and characterization of $[Gd(dtpa)]^{2-}$ intercalated layered double hydroxide (LDH) nanomaterials. $[Gd(dtpa)]^{2-}$ (gadolinium(III) diethylene triamine pentaacetate) was transferred into LDH by anionic exchange. The intercalation of $[Gd(dtpa)]^{2-}$ into LDH was confirmed by X-ray diffraction for the new phase with the interlayer spacing of 3.5–4.0 nm and by FTIR for the characteristic vibration peaks of $[Gd(dtpa)]^{2-}$. The morphology of the nanoparticles was influenced by the extent of $[Gd(dtpa)]^{2-}$ loading, in which the poly-dispersity quality decreased as the $[Gd(dtpa)]^{2-}$ loading was increased. Compared with the morphology of the original Mg_2Al–Cl–LDH nanoparticles (hexagonal plate-like sheets of 50–200 nm), the modified LDH–Gd(dtpa) nanoparticles are bar-like with a width of 30–60 nm and a length of 50–150 nm. LDH–Gd(dtpa) was expected to have an increased water proton magnetic resonance relaxivity due to the intercalation of $[Gd(dtpa)]^{2-}$ into the LDH interlayer that led to slower molecular anisotropic tumbling compared with free $[Gd(dtpa)]^{2-}$ in solution. Indeed, LDH–nanoparticle suspension containing ≈ 1.6 mM $[Gd(dtpa)]^{2-}$ exhibits a longitudinal proton relaxivity r_1 of $\approx 16\ mM^{-1}s^{-1}$ and a transverse proton relaxivity r_2 of $\approx 50\ mM^{-1}s^{-1}$ at room temperature and a magnetic field of 190 MHz, which represents an enhancement four times (r_1) and 12 times (r_2) that of free $[Gd(dtpa)]^{2-}$ in solution under the same reaction conditions. We have thus tailored LDH–nanoparticles into a novel contrast agent with strong relaxivity, promising for great potential applications in magnetic resonance imaging.

Keywords: clays · contrast agents · hydroxides · nanotechnology · proton relaxivity enhancement

Introduction

Various Gd^{III} complexes have been developed as clinical contrast-enhancing agents in magnetic resonance imaging (MRI), as a tool for clinical diagnosis of organ and tissue abnormalities.[1–6] These complexes enhance the magnetic resonance longitudinal (T_1) and transverse (T_2) relaxation of the nearby water protons, leading to signal enhancement as observed in MRI. Increasing the level of detection of abnormal organs and tissues in diagnostic MRI is closely linked to the improvement of the water proton relaxivities of these Gd^{III} complexes. A typical example is $[Gd(dtpa)(H_2O)]^{2-}$ (gadolinium(III) diethylene triamine pentaacetate hydrate), as shown in Figure 1. The improvement can be achieved by elongating the rotational correlation lifetime of the nuclear ions[1,7] and optimizing the water exchange rate.[8–14] Currently, considerable effort is being dedicated to designing new ligand structures, including macrocyclic, polymeric and dendritic frameworks with various functional groups, such as carboxylates, aminos/iminos, phosphates, to increase the rotational correlation lifetime.[1,6,7] Some macromolecular ligands have been designed to contain many Gd^{III} atoms and to have a relatively long molecular tumbling time and an optimal exchange rate of the coordinated water molecule (see Figure 1), leading to higher proton relaxivities.[1,7,9,10]

Recently, new efforts involving the incorporation of Gd^{III} cations into the framework of inorganic nanoparticles have

[a] Dr. Z. P. Xu, Prof. Dr. G. Q. Lu
ARC Centre for Functional Nanomaterials
School of Engineering
and
Australia Institute of Bioengineering and Nanotechnology
The University of Queensland
Brisbane, QLD 4072 (Australia)
Fax: (+61) 7-33463973
E-mail: maxlu@uq.edu.au

[b] Dr. N. D. Kurniawan, Prof. Dr. P. F. Bartlett
Queensland Brain Institute
The University of Queensland
Brisbane, QLD 4072 (Australia)

[c] Dr. N. D. Kurniawan
Centre for Magnetic Resonance
The University of Queensland
Brisbane, QLD 4072 (Australia)

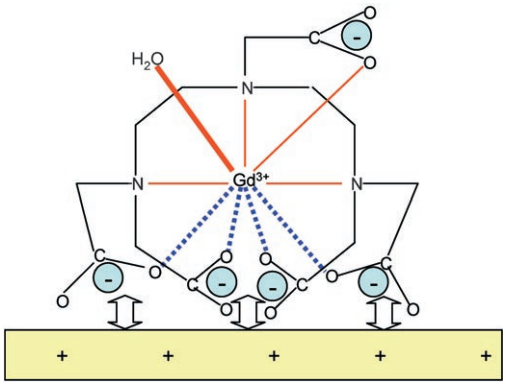

Figure 1. Schematic of possible configuration and interactions between $[Gd(dtpa)]^{2-}$ and the positive hydroxide layer.

been reported to improve the relaxivities.[15–17] For example, Gd^{III} cations were trapped in the supercage of NaY zeolite[15] or incorporated into a mesoporous silica framework.[16] In both cases, their magnetic resonance relaxivities increased 3–5 times in the longitudinal axis and 10–20 times in the transverse axis in comparison with those of free $[Gd(dtpa)]^{2-}$ ions. In this work, we attempted a new way to enhance the relaxivities of Gd^{III}-complex contrast agents by intercalation into layered double hydroxide (LDH) nanoparticles. This method has indeed enhanced the longitudinal relaxivity by more than four times and the transverse relaxivity by up to 12 times, in relation to the free $[Gd(dtpa)]^{2-}$ solution.

LDHs are a group of anion-exchanging materials containing mixed metal hydroxide layer similar to brucite, $Mg(OH)_2$. In a brucite layer, each Mg^{2+} ion is octahedrally surrounded by six OH^- ions and the different octahedra share edges to form an infinite 2D layer. In hydrotalcite, $[Mg_6Al_2(OH)_{16}][CO_3{\cdot}4H_2O]$, a quarter of Mg^{2+} are replaced by Al^{3+}, which gives the brucite-like layers positive charges that are balanced by carbonate anions located in the interlayer region. The positively charge brucite-like layers ($[Mg_6Al_2(OH)_{16}]^{2+}$), interlayer anions and water molecules ($[CO_3{\cdot}4H_2O]^{2-}$) are held together via electrostatic interactions and hydrogen bonds to form a 3D structure.[18,19] In general, LDHs can be chemically expressed by a formula such as $[M^{2+}_{1-x}M^{3+}_x(OH)_2]^{x+}$ $[(A^{m-})_{x/m}{\cdot}nH_2O]^{x-}$, where M^{2+} represents any divalent cations such as Mg, Zn, Ni, Co, and Fe, M^{3+} represents any trivalent cations such as Al, Fe, and Cr, and A^{m-} represents the exchangeable anions, such as CO_3^{2-}, Cl^-, SO_4^{2-}, various organic anions and complex anions.

MgAl–LDH possesses physical properties which make it suitable as the carrier of $[Gd(dtpa)]^{2-}$ with potential for clinical use: i) MgAl–LDH has been shown to be a biocompatible material with low cytotoxicity;[20] ii) $[Gd(dtpa)]^{2-}$ can be readily intercalated into the LDH interlayer through a chemical exchange process. The chelation of Gd^{III} with DTPA minimizes its toxicity if it de-intercalates from LDH nanoparticles. This is different from the situation in NaY zeolite and mesoporous silica where the Gd^{III} metal ions are non-chelated, and thus potentially toxic; iii) the $[Gd(dtpa)]^{2-}$ intercalated LDH nanoparticles, like the polymeric macromolecules chelating with Gd^{III}, rotate much more slowly, which is expected to promote the relaxations of bound water protons; iv) the particle size and morphology of LDH nanoparticles can be well controlled during the preparation.[21] Therefore, in this paper, we intercalated various amounts of $[Gd(dtpa)]^{2-}$ [Gd(dtpa) hereafter] into Mg_2Al–LDH nanoparticles and investigated the subsequent effect on the water proton relaxivities.

Results and Discussion

Intercalation of $[Gd(dtpa)]^{2-}$ into the LDH interlayer: The intercalation of $[Gd(dtpa)]^{2-}$ into the Mg_2Al–LDH interlayer is evidenced by the XRD patterns as shown in Figure 2. Obviously, the major phase in each sample is attributed to Mg_2Al–Cl–LDH as the interlayer spacing ranges from 0.766 to 0.773 nm, identical to that reported elsewhere.[18,19] However, as marked in Figure 2 (#) for samples E–H, a broad diffraction at around 2–2.5° can be observed. This peak corresponds to an interlayer spacing of 3.5–4.0 nm, which could be attributed to the formation of the Mg_2Al–Gd(dtpa)–LDH phase. Simultaneously, the diffraction peaks belonging to the Mg_2Al–Cl–LDH phase become broader, as indicated by the increase in FWHM of peak (*003*) from 0.34 to 0.83° (Table 1). In addition, a small bump diffraction at 18–19° (+) in Figure 2 indicates a trace amount of brucite $[Mg(OH)_2]$ formed after hydrothermal treatment.[21]

The IR spectra illustrated in Figure 3 also indicate the intercalation of $[Gd(dtpa)]^{2-}$ into the interlayer. The characteristic IR peaks of $[Gd(H_2dtpa)]$ at 1591 and 1409 cm^{-1} (Figure 3), attributed to the asymmetrical and symmetrical COO stretching vibrations,[22,23] gradually intensify from sample A to H at 1599 and 1409 cm^{-1}, respectively. Some finger-printing IR peaks of $[Gd(H_2dtpa)]$ at around 1000 cm^{-1} can also be distinguished in samples E to H as shoulders. Apart from these, the feature IR peaks of Mg_2Al–LDH can be noted, including a broad band at 3450 cm^{-1} (ν_{OH}), a shoulder at 3000 cm^{-1} (ν_{OH} for O–H bond H–bound with CO_3^{2-}), a strong peak at 1365 cm^{-1} [due to $\nu(CO_3^{2-})$] and bands (780, 683, 551 and 447 cm^{-1}) below 1000 cm^{-1} (due to M–O vibrations and M-O-H bending).[19,24] In particular, the peak at 447 cm^{-1} is an unique evidence of 2:1 MgAl–LDH materials.[24] The relatively strong peak at 1365 cm^{-1} in samples A and C indicates considerable contamination of CO_3^{2-} due to the CO_2 capture during exchanging and washing, which also causes a shoulder at 3000–3100 cm^{-1}. Note that the shoulder becomes much broader in samples E–H (3200–2800 cm^{-1}), as in $[Gd(H_2dtpa)]$, due to more H-bonded O–H stretching vibrations that overlap with C–H stretching vibrations.

The elemental analysis shows that more $[Gd(dtpa)]^{2-}$ ions are intercalated into the LDH interlayer when more $[Gd(dtpa)]^{2-}$ ions are present in the exchange reaction. As can be seen in Table 1, the intercalation degree in LDH nano-

Table 1. Physical characters of Mg_2Al–Gd(dtpa)/Cl/CO_3–LDH.

Sample	Molecular formula	2[Gd]/[Al] ratio		FWHM [°]	Average particle size [nm]	PDI	ζ potential [mV]
		Added	Obsd				
A	$Mg^2Al(OH)_6[Gd(dtpa)]_{0.003}(Cl+{}^1/_2CO_3)_{0.99}\cdot n\,H_2O$	0.01	0.006	0.34	129	0.128	44.2
B	$Mg^2Al(OH)_6[Gd(dtpa)]_{0.012}(Cl+{}^1/_2CO_3)_{0.98}\cdot n\,H_2O$	0.05	0.024	0.38	133	0.141	46.0
C	$Mg^2Al(OH)_6[Gd(dtpa)]_{0.038}(Cl+{}^1/_2CO_3)_{0.92}\cdot n\,H_2O$	0.20	0.076	0.60	106	0.100	32.1
D	$Mg^2Al(OH)_6[Gd(dtpa)]_{0.065}(Cl+{}^1/_2CO_3)_{0.85}\cdot n\,H_2O$	0.40	0.130	0.52	91	0.120	27.2
E	$Mg^2Al(OH)_6[Gd(dtpa)]_{0.099}(Cl+{}^1/_2CO_3)_{0.80}\cdot n\,H_2O$	0.80	0.198	0.60	83	0.145	25.6
F	$Mg^2Al(OH)_6[Gd(dtpa)]_{0.110}(Cl+{}^1/_2CO_3)_{0.78}\cdot n\,H_2O$	1.00	0.220	0.76	112	0.266	22.8
G	$Mg^2Al(OH)_6[Gd(dtpa)]_{0.150}(Cl+{}^1/_2CO_3)_{0.70}\cdot n\,H_2O$	1.50	0.300	0.80	151	0.273	22.1
H	$Mg^2Al(OH)_6[Gd(dtpa)]_{0.173}(Cl+{}^1/_2CO_3)_{0.65}\cdot n\,H_2O$	2.00	0.346	0.83	185	0.423	22.0

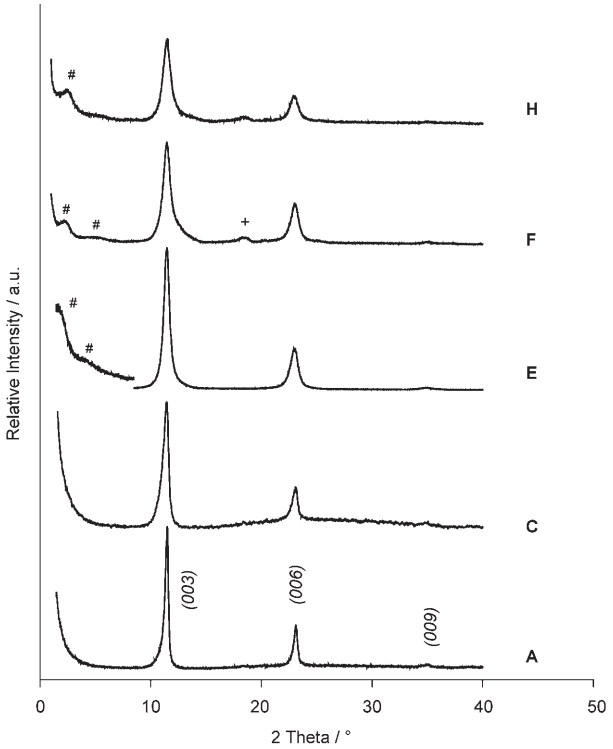

Figure 2. XRD pattern evolution of Mg_2Al-LDHs with different loadings of $[Gd(dtpa)]^{2-}$. Samples A, C, E, F, H contain 0.05, 0.55, 1.63, 1.71, 2.70 mM $[Gd(dtpa)]^{2-}$ (see Table 1).

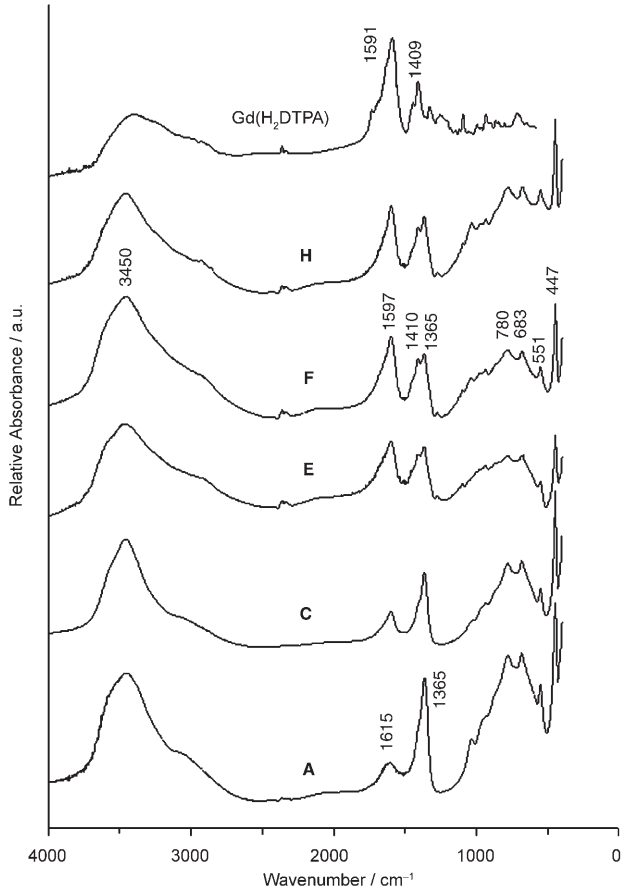

Figure 3. FTIR spectral evolution of Mg_2Al–LDH with different loadings of $[Gd(dtpa)]^{2-}$.

particles, that is, 2[Gd]/[Al] ratio, gradually increases from 0.006 to 0.346 for samples A to H. However, the intercalation or exchange is relatively incomplete. For example, only about 35% of anions are exchanged even if 200% equivalent $[Gd(dtpa)]^{2-}$ are available for the exchange in sample H (Table 1). One possible reason for this incomplete exchange is the contamination of CO_3^{2-} that occupy some sites and are difficult to replace. The determinant factor for the lower loading of $[Gd(dtpa)]^{2-}$ into Mg_2Al–LDH, however, is largerly a result from its specific size and charge. As estimated from the crystallography data, the dimension of $[Gd(dtpa)]^{2-}$ is approximately 1.3 nm.[25] Therefore, even with the assumption that $[Gd(dtpa)]^{2-}$ packing in the LDH gallery is a bilayer, the closely packed $[Gd(dtpa)]^{2-}$ bilayer has only resulted in a negative charge density of 2.4 e nm^{-2} ($2e \times 2/1.3^2$ nm^2), much less than that required to compensate for the positive charges in an Mg_2Al–hydroxide layer (4.0 e nm^{-2}).[18] Therefore about 40% equivalent small anions (such as Cl^-, CO_3^{2-}) must be simultaneously intercalated to compensate for the excess positive charge in the hydroxide layer. This reasoning means that the theoretical exchange degree is 60%, that is, 2[Gd]/[Al] can only reach 0.60 at most. Therefore, the small anions (Cl^- and CO_3^{2-}) have to be accompanied in the sample layer to balance the charges. Seemingly, this Mg_2Al–$[Gd(dtpa)]^{2-}/Cl^-/CO_3^{2-}$–LDH hybrid phase becomes detectable by XRD when the 2[Gd]/[Al] ratio, that is, the exchange degree, reaches 0.2.

Size and morphology of Mg_2Al–$[Gd(dtpa)]^{2-}$–LDH nanoparticles: After the hydrothermal treatment, the obtained

$[Gd(dtpa)]^{2-}$–LDH aqueous suspensions generally appear quite homogeneous. As shown for the particle size distribution in Figure 4, most particles in these samples are in the

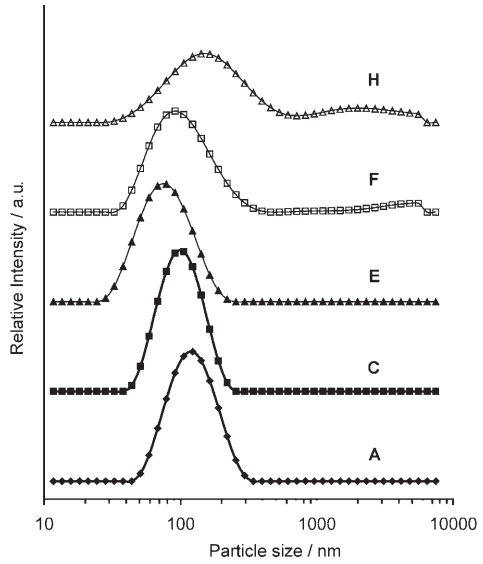

Figure 4. Particle size distribution of as-prepared suspension samples measured with photon correlation spectroscopy (PCS).

range of 40–200 nm. The size distribution is relatively narrow, as indicated by the small polydispersion index (PDI) (from 0.100 to 0.423 in Table 1). Overall, the average hydrodynamic particle size decreases from 129 to 83 nm (sample A to E) and then increases to 185 nm (sample E to H) when more $[Gd(dtpa)]^{2-}$ are intercalated. However, the polydispersibility of as-prepared Gd(dtpa)–LDH suspensions becomes worse as the PDI increases from 0.100 to 0.423 in the same ordering. In fact, some aggregates in the suspension of sample H were visible. This may be related to the adsorption of some $[Gd(dtpa)]^{2-}$ ions on the LDH nanoparticle surface. As shown in Table 1, the zeta potential of these LDH nanoparticle suspensions gradually decreases from 46 to 22 mV for samples A to H, which could be resulted from more $[Gd(dtpa)]^{2-}$ anions dynamically located on the surface than Cl^-/CO_3^{2-} ions due to its relatively strong interactions (Figure 1).[26] These surface $[Gd(dtpa)]^{2-}$ ions have not only led to a low zeta potential, but also caused LDH nanoparticles to aggregate to some degree, as observed in suspension samples F to H.

The morphology of unmodified Mg_2Al–Cl–LDH nanoparticles prepared by using a similar method is hexagonal platelike sheets, with a lateral dimension of 50–200 nm, as shown in Figure 5a.[21,27] However, in samples F–H, most nanoparticles have a rod-like morphology, while others form irregular thin plates (Figure 5b). In contrast, samples A and B have fewer rod-like nanoparticles but more hexagonal platelets. The nanorods are quite uniform, being 30–60 nm wide and 50–150 nm long, and presumably assigned to the formation of Mg_2Al–$[Gd(dtpa)]^{2-}/Cl^-/CO_3^{2-}$–LDH hybrid crystals. Under normal conditions, Mg_2Al–Cl/CO_3–LDH crystallites grow preferentially along the *a* and *b* axes, resulting in hexagonal platelets.[21,27] However, this growth preference could be altered in the presence of bulky $[Gd(dtpa)]^{2-}$ anions. Instead, $[Gd(dtpa)]^{2-}$ complex anions probably direct the growth along the *c* axis and thus induce the formation of the nanorod crystals, as in the case of dodecylbenzene sulfonate in Mg_2Al–LDH.[28]

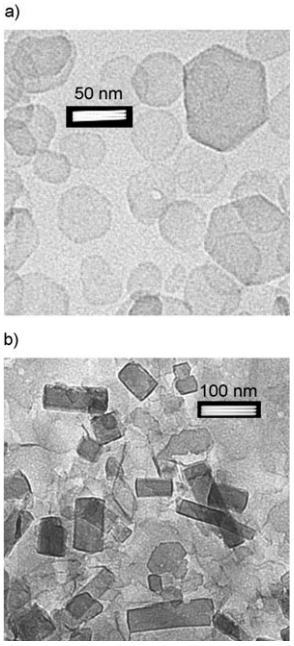

Figure 5. TEM images of typical Mg_2Al–Cl–LDH (a) and Mg_2Al-$[Gd(dtpa)]^{2-}$–LDH nanoparticles (b, sample F).

Proton relaxivities r_1 and r_2: The longitudinal and transverse relaxation times, T_1 and T_2, were measured for all samples that were freshly prepared in stable suspensions, as described in the Experimental section. The T_1 and T_2 times of all samples and the proton relaxivities, r_1 and r_2 of samples E to H are listed in Table 2. Figure 6 presents the typical plots of $1/T_1$ and $1/T_2$ versus Gd(dtpa) millimolarity in a series of diluted suspensions, using samples F (■) and H (□) as examples, to determine the relaxivities r_1 and r_2. Note

Table 2. Proton relaxation parameters of Mg_2Al–$Gd(dtpa)/Cl/CO_3$–LDHs at room temperature and a magnetic field of 190 MHz.

Sample	[Gd] [mM]	T_1 [ms]	T_2 [ms]	r_1 [$mM^{-1}s^{-1}$]	r_2 [$mM^{-1}s^{-1}$]
A	0.05	743	68.2		
B	0.19	298	72.3		
C	0.55	96	29.8		
D	0.97	76	19.7		
E	1.63	36	13.1	16.1	50.0
F	1.71	34	12.4	15.7	47.5
G	2.33	45	10.5	9.5	47.1
H	2.70	54	8.8	6.4	44.8

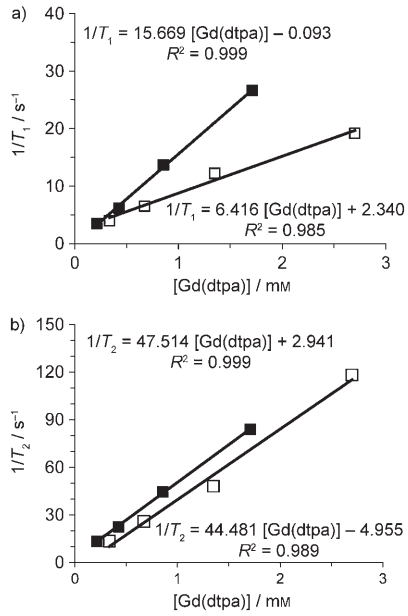

Figure 6. Proton relaxivities r_1 and r_2 of samples F (■) and H (□).

that the longitudinal relaxivity r_1 (6.4–16.1 $mM^{-1}s^{-1}$) and the transverse relaxivity r_2 (44.8–50.0 $mM^{-1}s^{-1}$) of these samples are much larger than those of $[Gd(dtpa)]^{2-}$ in free solution (3.4 and 4.2 $mM^{-1}s^{-1}$ at room temperature and 190 MHz), respectively. It is also noted that when the $[Gd(dtpa)]^{2-}$ loading in LDH is increased over 1.7 mM, the r_1 value significantly decreases from 16 to about 6 $mM^{-1}s^{-1}$ (Table 2). Consistent with this observation, a more obvious relationship in the current loading range (0.05 to 2.70 mM, Table 2) is presented in Figure 7 for all samples. When $1/T_1$ and $1/T_2$ of all samples are plotted against Gd(dtpa) concentration, a linear

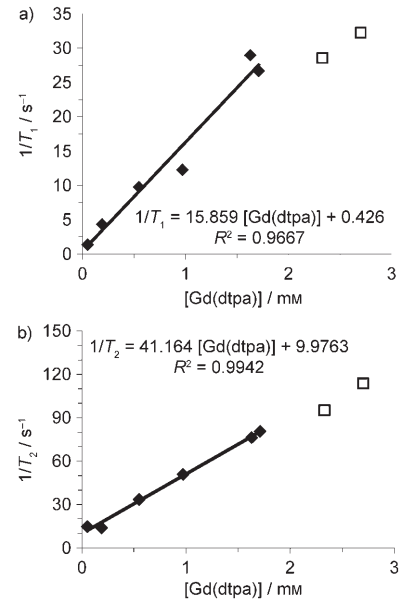

Figure 7. Proton relaxivities r_1 and r_2 of Mg_2Al–$[Gd(dtpa)]^{2-}$–LDH (for all samples).

relationship is obtained at [Gd(dtpa)] below 1.7 mM. The slopes, that is, the average relaxivities r_1 and r_2 of these samples are 15.8 and 41.2 $mM^{-1}s^{-1}$, respectively, identical to those of samples E and F if experimental measurement errors and data treatment errors are considered. These analyses indicate that the proton relaxivities can be enhanced more than four times in the longitudinal axis and 10–12 times in the transverse axis by intercalating $[Gd(dtpa)]^{2-}$ ions into the LDH interlayer, as compared with those in free solution. At [Gd(dtpa)] above 1.7 mM (Gd wt% in LDH = ≈5%), a decrease in relaxivities r_1 and r_2 is noticeable. A similar decrease in relaxivities was also reported for Gd^{III}-doped mesoporous silica at Gd loading over 2.3% in w/w.[16] The decrease in relaxivity is presumably a result of the increase in dipole–dipole interaction of the adjacent nuclear Gd^{III} species that shortens the electronic relaxation, that is, shortens the proton relaxavities[15,16] with the decrease of water molecules available for each $[Gd(dtpa)]^{2-}$ in the interlayer being another relevant factor, as addressed in the following section.

Enhancement mechanism: The relaxivity enhancement of Gd^{III} chelated with macromolecules or incorporated into nanoparticles has been discussed in detail elsewhere.[1,7] The major factors for this enhancement include: i) enlongation of the rotational correlation lifetime of Gd^{III} species; ii) suitable water exchange rate; and iii) small electron–nuclear spin distance. In the case of Gd(dtpa)-intercalated LDHs, these factors have presumably affected the relaxivities to some degree, in comparison with the free $[Gd(dtpa)]^{2-}$ ions.

Obviously, most $[Gd(dtpa)]^{2-}$ ions are confined in the LDH interlayer and thus the ionic motions (e.g. rotational and transitional) within the interlayer are much more restricted, in particular, $[Gd(dtpa)]^{2-}$ ions are supposed to anchor onto the hydroxide layer through the electrostatic attraction and hydrogen bonds, as schematically drawn in Figure 1. Moreover, the LDH–Gd(dtpa) nanorods (Figure 5b), 30–60 nm wide and 50–150 nm long, tumble much more slowly than the free $[Gd(dtpa)]^{2-}$ ions.[1] The restricted movement of $[Gd(dtpa)]^{2-}$ in the interlayer and very slow nanoparticle tumbling are expected to lead to a longer rotational correlation time, thus increasing the relaxivities.

The exchange rate of water protons in $[Gd(dtpa)]^{2-}$, including the water exchange rate and the prototropic exchange rate,[8] may have negative contribution to enhance the relaxivities. For example, the number of water molecules (n) in Table 1 is about 1.5 for all samples and thus the available water molecule number per $[Gd(dtpa)]^{2-}$ in the interlayer decreased from 500 to 8 for samples A to H. Therefore, the small water number per $[Gd(dtpa)]^{2-}$ in samples G and H (8–10) may decrease r_1 relaxivity.[15] In zeolite nanoparticles, a typical number of 15–100 water molecules per Gd ion seems to be sufficient to provide a similar level of water exchange rate as in free solution.[15]

The main interaction holding $[Gd(dtpa)]^{2-}$ anions within the interlayer is the electrostatic attraction between the anions and the positively charged hydroxide layers,[18] to-

gether with hydrogen bonds between them. As schematically shown in Figure 1, the attractions would pull the coordinated O atoms (in COO^- groups) away from the nuclear centre (Gd^{3+}) and thus weaken these $Gd^{3+}\cdots O$ coordination bonds (dashed blue lines in Figure 1). This bond weakening could be compensated for by the strengthening of the CO bond in the same COO^- group, as evidenced by the blue shift of the characteristic IR peak from 1591 cm^{-1} in [Gd((H_2dtpa)] to 1599 cm^{-1} in LDH (asymmetrical COO^- stretching vibration). As another consequence, the $Gd^{3+}\cdots OH_2$ bond (bold red line) as well as other coordination bonds (thin red lines) would be strengthened. The strengthening of the $Gd^{3+}\cdots OH_2$ bond, that is, the shortening of the electron-nuclear spin distance, would amplify the proton relaxivities about six times.[1]

Conclusion

In conclusion, $[Gd(dtpa)]^{2-}$ has been partially intercalated into Mg_2Al–LDH nanoparticles by anionic exchange and hydrothermal treatment. The interlayer spacing (3.5–4.0 nm) obtained from XRD data suggests that $[Gd(dtpa)]^{2-}$ anions are packed in a bilayer model in the LDH interlayer. Such close packing of $[Gd(dtpa)]^{2-}$ still needs some small anions (Cl^- and CO_3^{2-}) together to compensate for the positive charges in the hydroxide layers due to the relatively large size of $[Gd(dtpa)]^{2-}$. The Mg_2Al–$[Gd(dtpa)]^{2-}/Cl^-/CO_3^{2-}$–LDH hybrid nanocrystals are morphologically rod-like, 30–60 nm wide and 50–150 nm long. Intercalation of $[Gd(dtpa)]^{2-}$ into the LDH interlayer enhances the proton relaxivities more than 4 times in the longitudinal axis and up to 12 times in the transverse axis, although high loading of $[Gd(dtpa)]^{2-}$ results in relatively small relaxivities. It is found that the major contribution to this enhancement comes from the increase in the rotational correlation lifetime of nuclear species while the shortening of the electron-nuclear spin distance may also contribute to a minor extent.

Experimental Section

Preparation of $[Gd(dtpa)]^{2-}$-containing layered double hydroxide nanoparticles: Layered double hydroxides (LDHs) were prepared by co-precipitation, anion exchange and hydrothermal treatment. In brief, the precursor $[Mg_2Al(OH)_6Cl]\cdot x H_2O$ was prepared by quickly adding (within 5 s) a salt solution mixture (10 mL) containing $MgCl_2$ (3.0 mmol) and $AlCl_3$ (1.0 mmol) into a NaOH solution (40 mL, 0.15 M, just enough to form Mg_2Al–LDH) to co-precipitate under vigorous stirring, followed by 10-minute stirring within a reactor isolated from air. The $[Mg_2Al(OH)_6Cl]\cdot x H_2O$ slurry was obtained via a centrifuge separation and then manually dispersed in a $[Na_2Gd(dtpa)]$ solution (40 mL) at a designated concentration for the anionic exchange (Table 1). The exchange was allowed to continue for 1 h under vigorous stirring at room temperature. After separating and washing once with deionized water, the Gd(dtpa)-containing LDH slurry was again dispersed in deionized water (40 mL), followed by hydrothermal treatment in an autoclave at 100 °C for 16 h, giving rise to a stable homogeneous LDH suspension in most cases. As-prepared suspensions generally have a pH of 8.0 and an Mg_2Al–Gd(dtpa)/Cl/CO_3–LDH concentration of 0.4–0.5 % in w/w as the LDH yield of 60±5 % has been calculated from the inductively coupled plasma (ICP) data as well as the LDH mass collected from suspensions. In particular, Gd as well as Mg and Al concentrations in the suspensions were determined by the ICP (Tables 1 and 2).

Characterization of Gd–DTPA–LDH materials: X-ray diffraction patterns were collected on a glass plate containing a thin layer of LDH hybrid materials at a scanning rate of 1.2° per minute with an interval of 0.02° in each step from $2\theta=1°$ to $2\theta=40°$ with $Cu_{K\alpha}$ radiation ($\lambda=0.15418$ nm) on a Bruker D8 Advance Research X-ray diffractometer by software Diffrac^{plus} Evaluation Package Version 11.0. The X-ray diffraction intensity varied within few thousand cps. Infrared spectra were collected on a Perkin-Elmer 2000 FTIR after 40 scans within 4000–400 cm^{-1} at a resolution of 4 cm^{-1} by measuring the IR absorbance of KBr disc that contains 1–2 wt % of sample. Photon correlation spectroscopy (PCS, Nanosizer Nano ZS, MALVERN Instruments) was used to analyze the particle size distribution of LDH suspensions from 0.6 nm to 6000 nm, in which the peak position (regarded as the average hydrodynamic particle size in the paper) and the polydispersion index (PDI) were automatically generated. The transmission electron microscopic images were obtained on a JEOL JSM-2010 transmission electron microscope (TEM) at an acceleration voltage of 200 kV. For TEM imaging, the freshly collected LDH nanoparticles were dispersed in alcohol with ultrasonication for 20 min, after which a droplet was placed on a copper grid coated with carbon film. In addition, the metal contents of suspension samples were determined by inductively coupled plasma and atomic emission spectroscopy (ICP-AES) on a Varian Vista Pro.

Water proton relaxivity measurement: The longitudinal and transverse relaxation times, T_1 and T_2, of water protons in the as-prepared Gd(dtpa)–LDH suspensions were measured at 190 MHz with a Bruker Biospect 4.6T/20 MR spectrometer at room temperature. The samples were aliquoted into 100 μL eppendorf tubes and held using 1 % agarose. T_1 relaxation times were measured either using the Fast-Imaging with Steady Precession (FISP) method[29] where TR/TE = 3.2/1.6 ms, flip angle = 60°, 40 τ_1 delay values of 40–3800 ms, or using a multi-point inversion recovery method using 8–16 τ_1 delay values of 17–8000 ms. T_2 relaxation times were measured using the Multi-Spin-Multi-Echo (MSME) method[30] employing a Carr-Pucell-Meiboom-Gill sequence (TR/TE = 5000/11 ms with 16 echos). The longitudinal (r_1) and transverse (r_2) relaxivities of a sample were determined by plotting the values of $1/T_1$ and $1/T_2$ versus the Gd(DTPA) millimolar concentration of a series of diluted suspensions of the same sample. In comparison, free $[Gd(dtpa)]^{2-}$ in solution was also measured in the relaxation times T_1 and T_2, which resulted in r_1 and r_2, respectively, under the same conditions (Table 2).

Acknowledgement

The work is produced as part of the activities of the ARC Centre for Functional Nanomaterials funded by the Australia Research Council under its Centre of Excellence Scheme. N.D.K. is grateful for the support of Dr. E. J. Coulson (Queensland Brain Institute) and Eijkman/BPPT while conducting his work.

[1] P. Caravan, J. J. Ellison, T. J. McMurry, R. B. Lauffer, *Chem. Rev.* **1999**, *99*, 2293.
[2] D. Delbeke, C. W. Pinson, *J. Hepatobiliary Pancreat. Surg.* **2004**, *11*, 4.
[3] J. C. C. Moon, S. K. Prasad, *Curr. Cardiol. Rev.* **2005**, *7*, 39.
[4] H. Degani, M. Chetrit-Dadiani, L. Bogin, E. Furman-Haran, *Thromb. Haemostasis* **2003**, *89*, 25.
[5] R. Sanjay, P. Martin, *Cardiol. Clin.* **2002**, *20*, 501.
[6] H. Kobayashi, M. W. Brechbiel, *Adv. Drug Delivery Rev.* **2005**, *57*, 2271.
[7] E. Toth, L. Helm, A. E. Merbach in *Chemistry of Contrast Agents in Medical Magnetic Resonance Imaging* (Ed.: A. E. T. Merbach), Wiley, Chichester, **2001**, p. 45.

[8] S. Aime, M. Botta, M. Fasano, E. Terreno, *Acc. Chem. Res.* **1999**, *32*, 941.
[9] J. L. Turner, D. Pan, R. Plummer, Z. Chen, A. K. Whittaker, K. L. Wooley, *Adv. Funct. Mater.* **2005**, *15*, 1248.
[10] D. M. Doble, M. Botta, J. Wang, S. Aime, A. Barge, K. N. Raymind, *J. Am. Chem. Soc.* **2001**, *123*, 10758.
[11] M. Woods, M. Botta, S. Avedano, J. Wang, A. D. Sherry, *Dalton Trans.* **2005**, 3829.
[12] Z. Jaszberenyi, A. Sour, E. Toth, M. Benmelouka, A. E. Merbach, *Dalton Trans.* **2005**, 2713.
[13] D. A. Fulton, M. O'Halloran, D. Parker, K. Senanayake, M. Botta, S. Aime, *Chem. Commun.* **2005**, 474.
[14] R. Ruloff, E. Toth, R. Scopelliti, R. Tripier, H. Handel, A. E. Merbach, *Chem. Commun.* **2002**, 2630.
[15] C. Platas-Iglesias, L. Vander Elst, W. Zhou, R. N. Muller, C. F. G. C. Geraldes, T. Maschmeyer, J. A. Peters, *Chem. Eur. J.* **2002**, *8*, 5121.
[16] Y.-S. Lin, Y. Hung, J.-K. Su, R. Lee, C. Chang, M.-L. Lin, C.-Y. Mou, *J. Phys. Chem. B* **2004**, *108*, 15608.
[17] G. A. Pereira, D. Ananias, J. Rocha, V. S. Amaral, R. N. Muller, L. Vander Elst, E. Toth, J. A. Peters, C. F. G. C. Geraldes, *J. Chem. Mater.* **2005**, *15*, 3832.
[18] P. S. Braterman, Z. P. Xu, F. Yarberry in *Handbook of Layered Materials* (Eds.: S. M. Auerbach, K. A. Carrado, P. K. Dutta), Marcel Dekker, New York, **2004**, p. 373.
[19] F. Cavani, F. Trifiro, A. Vaccari, *Catal. Today* **1991**, *11*, 173.
[20] S. Y. Kwak, Y. J. Jeong, J. S. Park, J. H. Choy, *Solid State Ionics* **2002**, *151*, 229.
[21] Z. P. Xu, G. Stevenson, C.-Q. Lu, G. Q. M. Lu, P. Bartlett, P. Gray, *J. Am. Chem. Soc.* **2006**, *128*, 36.
[22] Z. P. Xu, P. S. Braterman in *Dekker Encyclopedia of Nanoscience and Nanotechnology* (Eds.: J. A. Schwars, C. I. Contescu, K. Putyera), Marcel Dekker, New York, **2004**, p. 3387.
[23] W. W. Simons, *The Sadtler Handbook of Infrared Spectra*, Sadtler Research Laboratories, Pennsylvania, **1978**.
[24] M. J. Hernandez-Moreno, M. A. Ulibarri, J. L. Rendon, C. J. Serna, *Phys. Chem. Miner.* **1985**, *12*, 34.
[25] H. Gries, H. Miklautz, *Physiol. Chem. Phys. Med. NMR* **1984**, *16*, 105.
[26] R. J. Hunter, *Zeta Potential in Colloid Science: Principles and Applications*, Academic Press, London, **1988**.
[27] H. Cai, A. C. Hillier, K. R. Franklin, C. C. Nunn, M. D. Ward, *Science* **1994**, *266*, 1551.
[28] Z. P. Xu, P. S. Braterman, *J. Mater. Chem.* **2003**, *13*, 268.
[29] A. P. Crawley, R. M. Henkelman, *Magn. Reson. Med.* **1988**, *7*, 23.
[30] J. D. De Certaines, W. M. M. J. Bovee, F. Podo, *Magnetic Resonance Spectroscopy in Biology and Medicine*, Pergamon, New York, **1992**.

Received: April 24, 2006
Revised: August 23, 2006
Published online: December 22, 2006

